Energy 141 (2017) 2321–2336

Contents lists available at ScienceDirect

Energy

journal homepage: www.elsevier.com/locate/energy

Modeling and simulation of a desiccant assisted solar and geothermal air conditioning system

Arne Speerforck [a, *], Jiazhen Ling [b], Vikrant Aute [b], Reinhard Radermacher [b], Gerhard Schmitz [a]

[a] Hamburg University of Technology, Institute of Engineering Thermodynamics, Denickestr. 17, 21073, Hamburg, Germany
[b] Center for Environmental Energy Engineering, 4164, Glenn Martin Hall Bldg., College Park, MD, USA

ARTICLE INFO

Article history:
Received 6 September 2017
Received in revised form
3 November 2017
Accepted 26 November 2017
Available online 5 December 2017

Keywords:
Desiccant Wheel
Borehole Heat Exchanger
Solar Energy
Air Conditioning
Simulation
LCCP

ABSTRACT

In this study, we investigated a desiccant assisted air conditioning system that includes borehole heat exchangers for direct cooling and solar energy for desiccant regeneration. We developed a system model and ran simulations of this model for five cities in the United States. Our research shows that the system can provide sufficient latent and sensible cooling throughout the cooling period. Depending on the location, a maximum Seasonal Energy Efficiency Ratio of up to 7.66 (kW/kW) is achieved. We further investigated the utilization of borehole heat exchangers within a desiccant assisted hybrid air conditioning system by comparing their energetic, economic and environmental performance to a vapor compression chiller that utilizes R410A as refrigerant. We found that electricity savings of more than 50% and CO_2 equivalent emission savings of up to 91% are possible, while the geothermal system is not cost competitive at most of the investigated locations.

1. Introduction

Worldwide sales of air conditioning devices increased considerably during recent years [1]. This trend is predicted to continue in future, mainly driven by income growth in hot regions and even increased by global warming [2]. Within a few decades, researchers predict a near universal saturation with air conditioning devices for all warm areas. Today in the United States (a high-income country with cooling demand), 87% of households use air conditioning devices [3]. Accordingly, research efforts to lower the electricity demand related to air conditioning remain important in the context of global emission control.

To provide comfortable room conditions, air conditioning appliances are required to remove sensible and latent loads. It is common practice to cool the air below dew point temperature for moisture removal; dehumidification and cooling are coupled within this process. Desiccant dehumidification offers a possibility to separate moisture removal from sensible cooling. In so-called hybrid air conditioning systems, the desiccant wheel handles the latent load while a closed loop cooling cycle removes the sensible loads. This leads to multiple benefits regarding the overall process [4]. We can significantly reduce the load imposed on the cooling cycle by using desiccant dehumidification in combination with a heat recovery unit. Additionally, cold water can be supplied at higher temperature levels, which increases the efficiency of most cycles used for cold water generation. However, to provide a continuous process, a hot air flow to regenerate the desiccant must be provided. Various configurations of hybrid systems have been tested by different researchers. Solar energy [5,6], heat supplied by a geothermal well [7], waste heat of a CHP engine [8,9] or heat rejected through the condenser of a vapor compression cycle (VCC) [10,11] were used to regenerate the desiccant wheel. The most common choice for the closed loop cooling cycle are VCCs [6,9], whereas also thermally driven chillers were tested [12,13]. Due to the higher cold water temperature level, the usage of shallow geothermal energy for direct cooling is another possible alternative, if soil and climate conditions are suitable.

Eicker and Vorschulze [14] presented an experimental and model-based analysis of geothermal cooling for office buildings. In the study, borehole heat exchangers (BHXs) with a depth of 80 m were used to cool office buildings in Germany. They measured a maximum heat dissipation of 26 W/m, which was mainly limited

* Corresponding author.
E-mail address: arne.speerforck@tu-harburg.de (A. Speerforck).

https://doi.org/10.1016/j.energy.2017.11.151

by the heat transfer within in the building. Validated with the experimental data, they used a numerical model to study the suitability of direct geothermal cooling of office buildings at different locations. They concluded that geothermal heat exchangers can also be applied in warmer Mediterranean climates, even though the cooling capacity decreases with increasing soil temperature. They also reported that the ground temperature regenerates to between 1.5 °C and 0.5 °C above the undisturbed temperature after each daily operational cycle, and just a slight increase is determined during the simulated cooling period. Kaushal [15] published a review of various studies on earth-air heat exchangers and concluded that these can be a promising and economically-effective alternative for the space cooling of buildings. Electricity savings of 25–30% are identified as well achievable through the usage of earth-air heat exchangers. A limited number of studies investigated the coupling of desiccant dehumidification and geothermal cooling. Enteria et al. [16] and El-Agouz and Kabeel [17] simulated the integration of BHXs in desiccant evaporative cooling cycles. In a conceptual study for a single family house, Enteria et al. included a U-tube heat exchanger to provide further cooling after the supply air passed the evaporative cooler. They reported that the geothermal heat exchanger helps the system to cover peak loads. El-Agouz and Kabeel [17] used a geothermal heat exchanger to precool the supply air before it enters the evaporative cooler, which is used to finally cool down the air to the desired supply air temperature. Assuming a constant outlet temperature of the BHX, the authors tested different cycles under different ambient conditions. They showed that the hybrid system provides thermal comfort under the investigated conditions and provided iso-lines for the thermal COPs of the investigated system under different ambient conditions. A considerable decrease in supply air temperature is achieved through the usage of a geothermal cycle. Both studies provide limited information about the geothermal part. Casas and Schmitz [8] presented a hybrid system including a geothermal loop for direct cooling and a CHP engine for heat generation. The authors present experimental results for a stationary point and identified a high potential for primary energy savings. They reported that comfort conditions could not be maintained for some rooms of the investigated building during hotter days of the cooling period.

Using this work as a starting point, Speerforck and Schmitz [18] presented an experimental evaluation of a desiccant assisted air handling unit coupled to BHXs throughout a whole cooling period. The air handling unit supplies ventilation to a reference room, which is equipped with cooling ceilings to remove sensible loads. They measured a Seasonal Efficiency Rate of 6.6, which allows the temperature level to maintain a comfortable level within the reference room throughout the entire cooling period. However, the applicability and efficiency of such a system depends greatly upon climatic conditions. The experimental results therefore cannot be readily transferred to other locations.

This study aims to test the applicability of the mentioned concept at different locations. We used the object-oriented language Modelica® to develop a system model [19]. We used this model to simulate the system during the cooling period in five different cities within the United States. A solar thermal system is sized for each location to regenerate the desiccant wheel, while a geothermal system is sized to provide a comfortable room temperature. A parametric study was conducted to investigate the dependency of thermal comfort on borehole depth. To further evaluate the utilization of BHXs within the system, we compared them to a VCC from an energetic, economic and environmental perspective.

2. System layout and control

Fig. 1 shows the layout of the investigated system, which was built at Hamburg University of Technology [18]. The system can be broadly divided into the air handling unit, the hot and cold water circuit, as well as the reference room.

The air handling unit is designed as a hybrid system; exemplary state changes within the air handling unit are displayed in Fig. 2. The latent load is converted to sensible load by a desiccant wheel (1–2). Sensible cooling is then achieved through a heat recovery wheel and dry cooling coil (2–4). Extracted air from the room is used to regenerate the desiccant wheel. It is preheated in the heat recovery wheel (5–6) and finally heated to the required regeneration air temperature in the heating coil (6–7). The system is operated with balanced air flows and lithium chloride is used as desiccant. A bypass allows saving the electricity required to run the fans in case the desiccant wheel or the heat recovery wheel are not necessary under mild and dry outdoor conditions.

The air cooler, as well as the cooling ceilings, are supplied by vertical double U-tube BHXs. Three BHXs with a depth of 80 m were installed at the test facility. In this study number and length of the BHXs are varied for the different locations. Sufficient sensible cooling of the space is achieved through the cooling ceilings. Due to their large surface area of 85 m^2, a relatively high water supply temperature compared with traditional VCC is sufficient to meet the sensible cooling loads of the room. The hot water required for the regeneration of the desiccant wheel is supplied by flat plate solar collectors. We chose the respective area to meet the latent load of the different locations for this investigation, and we used a stratified thermal storage is used to balance demand and supply.

The reference room consists of four 20 feet (6 m) containers and exhibits an overall area of 56 m^2, with a height of 2.64 m. A schematic drawing of the room, as well as a picture of the actual facility, is displayed in Fig. 3. Note that just the upper four containers of the picture serve as the reference room. For the simulation, it is assumed that the four walls of the room point directly towards the four cardinal points as displayed by the compass in Fig. 3. All walls are insulated with a 10 cm layer of mineral wool, which is covered by thin steel plates. More detailed construction information can be found in Ref. [6], where an EnergyPlus model of the respective room was presented.

2.1. System control and load profiles

The bypass of the air handling unit is controlled in dependence on ambient conditions. The control strategy is based on the proposals of [10] and [20]. It is visualized in Fig. 4. Four different operational modes (OMs) are used. The different components, namely the desiccant wheel (DW), the air cooler (AC), the air heater (AH) and the heat recovery wheel (HRW) are activated according to Table 1. In the first mode, all components are bypassed and the fans are used to supply outdoor air to the conditioned space. The second mode is used as soon as dehumidification of the outdoor air is required. The trigger used to switch between the modes is an outdoor water content of 9 g/kg. For outdoor temperatures above 21 °C combined with a water content below 9 g/kg, the desiccant wheel is bypassed and the outdoor air is cooled by the heat recovery wheel as well as the cooling coil. The heat recovery wheel is activated if the room temperature is below ambient air temperature. If the outdoor temperature drops below 17.5 °C, the heat recovery wheel is used to transfer heat from the exhaust air to supply air. We set the limits according to the desired indoor conditions and the expected internal loads. The desired range for room

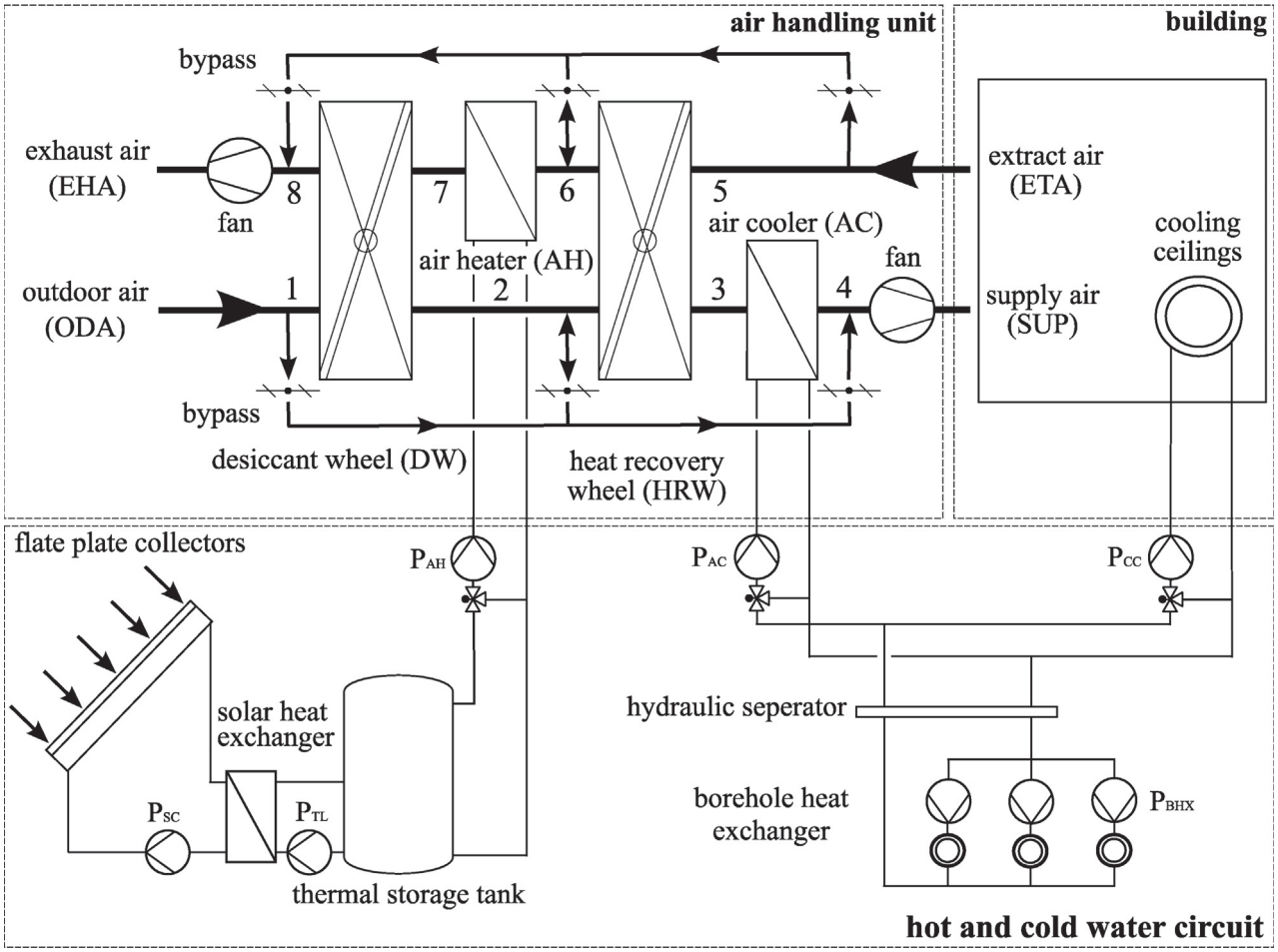

Fig. 1. Layout of the investigated system.

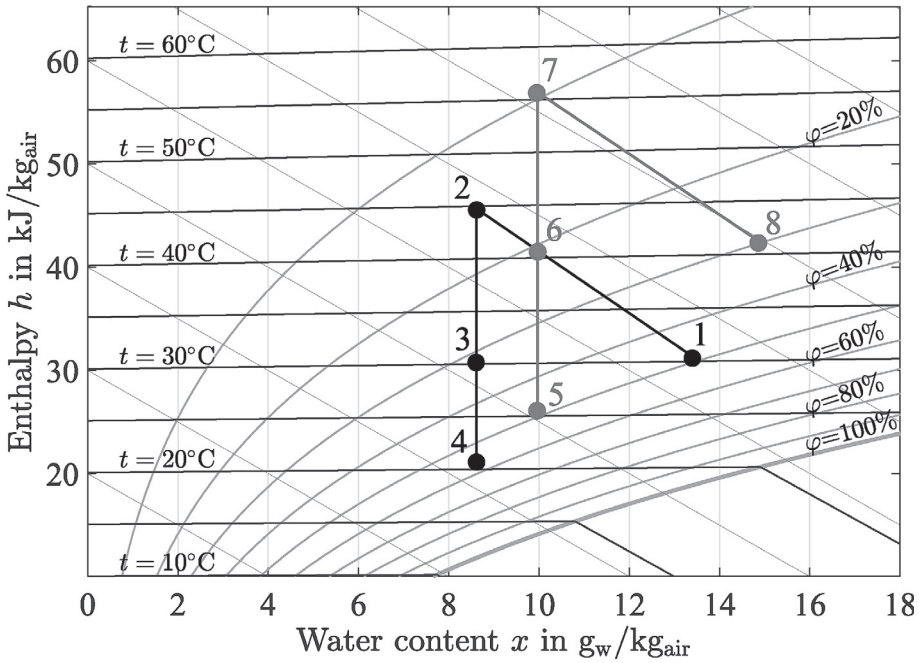

Fig. 2. Exemplary state changes within the air handling unit.

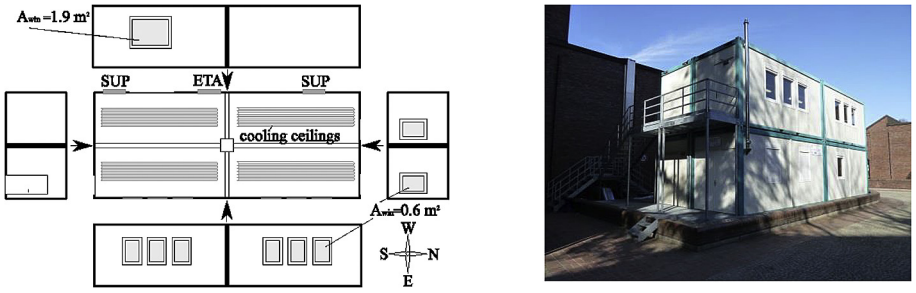

Fig. 3. Schematic drawing and actual configuration of reference room.

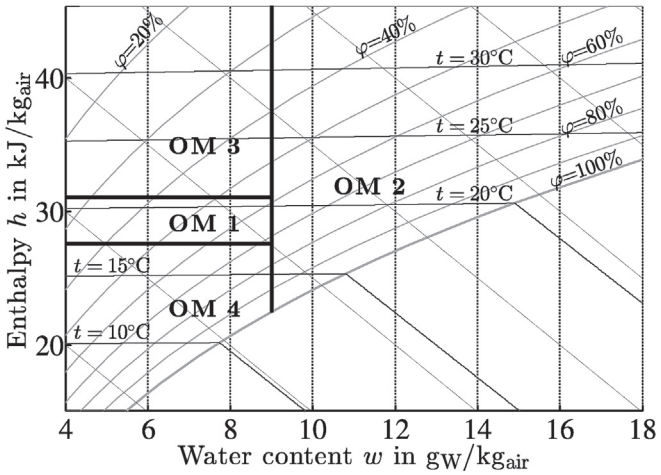

Fig. 4. Control strategy depending on ambient conditions.

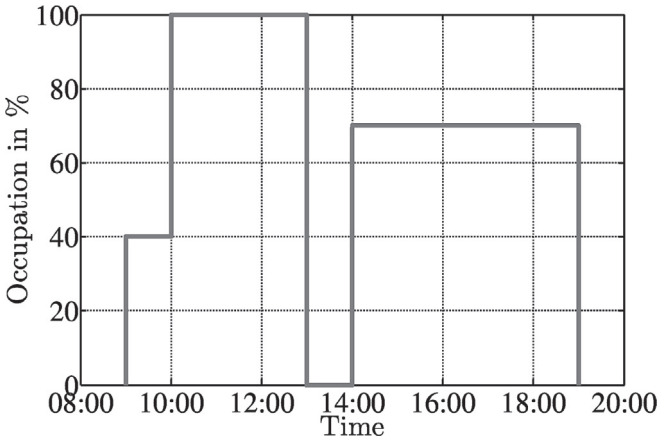

Fig. 5. Occupation profile of the reference room.

temperature is between 27 and 22 °C, while the system aims to keep room humidity ratio below 12 g/kg. These limits were determined according to ASHRAE standard 55 [21], assuming a metabolic rate of 1.1, a clothing level of 0.5 and an average air speed of 0.1 m/s. For the determination of the internal loads, it is assumed that the reference room is used as a classroom with 30 seats and the calculation follows the approach of [22]. We used a daily occupational profile similar to the mentioned study. The room has a varying occupancy between 9 a.m. and 7 p.m., and the respective profile is displayed in Fig. 5. The system is operated between 8:30 a.m. and 7:30 p.m. An occupant is assumed to add 55 W latent load and 65 W sensible load to space. Heat gain from lighting and other electronic appliances is assumed to be 10 W/m^2. The supply air ventilation rate is chosen based on [23] and fixed at 950 m^3/h. The supply air in dehumidification and cooling mode is set to be 21 °C for the temperature and 8.5 g/kg for the water content. The cooling ceilings are operated with a constant mass flow, the inlet temperature is controlled as a function of ambient temperature. To avoid condensation, the respective inlet temperature is always controlled to be at least 1.5 °C above the dew point temperature corresponding to the room air state.

2.2. Sizing procedure and simulation period

We investigated five cities within the continental United States for this study: Chicago, New York, Washington DC, San Diego and San Francisco. For San Diego, the system is simulated from June to October, for the other cities the system is simulated from May until September. The length of operating timeframe are chosen based on preliminary analyses of the weather data. To match the latent and sensible cooling demand for the different locations, the number and depth of the BHXs, as well as the solar collector area, are adjusted for each city. As the latent load is mainly handled by the desiccant wheel, the number of solar panels is increased until 95% of the operating time meets the comfort criterion ($w_{room} < 12$ g/kg). The size of the BHXs is increased in 10 m steps until the room temperature exceeds 27 °C during less than 5% of the operating hours. If the depth exceeds 100 m, the number of BHXs is increased and the process is repeated. However, if more than one

Table 1
Control of the air handling unit.

OM	Description	Ambient conditions		Active components			
		w(g$_W$/kg$_{air}$)	t (°C)	DW	HRW	AH	AC
OM 1	Fresh air	w < 9	t < 21	–	–	–	–
OM 2	Cooling + dehumidification	w > 9	–	x	x	x	x
OM 3	Cooling	w < 9	t > 21	–	(x)	–	x
OM 4	Heating	–	t < 17.5	–	x	–	–

BHX are used, all of them exhibit the same depth. In this way computational effort is reduced as just on BHX needs to be simulated. Just one cooling period is investigated, long-term warming of the soil (in case of an asymmetric load on the BHX for summer and winter) is not considered.

3. Modeling approach

We modeled all components of the proposed system using the object-oriented equation based modeling language Modelica®. The transient behavior of the system is mainly influenced by the BHXs, the building, as well as the solar thermal system. Accordingly, models which account for the dynamic behavior of these components are used. The air handling unit is considered as a quasi-steady state. TMY 3 weather data have been used for all different locations. All necessary data, such as average ambient temperatures or soil temperature profiles, were derived based on these data.

3.1. Borehole heat exchangers

The geothermal model is crucial to obtain an accurate performance prediction of the proposed system. Through varying cooling load of the building, as well as the shutdown of the system during night-time, the boundary conditions of the BHXs vary continuously. These changes and the respective short- and long-term transient response need to be represented by the model, while in a system simulation certain limits apply to the detail level of the component models. A suitable approach regarding this trade-off are the thermal resistance and capacity models provided for different BHXs in Ref. [24]. The BHX is divided into a discrete number of layers which will be explained in detail in the later sections. Per layer, the model assigns one heat capacity of the grouting material (C_g) to each of the four pipes of the double U-tube BHX. If the mass flow is equally distributed on each of the two pipes flowing down, the heat transfer problem is symmetric and the number of heat capacities required to describe the problem can be reduced; this leads to a reduced number of state variables required for the numerical integration. The problem can be described by a model configuration similar to a single U-tube heat exchanger as proposed in Ref. [25]. To reduce the computational effort, the temperature at the borehole wall is assumed to be uniform and can therefore be described by just one temperature node. This enables a one dimensional description of the surrounding soil. Heat conduction within the soil is modeled by connecting further capacitances and resistances to the borehole wall. Furthermore, vertical conduction between the modeled layers can be taken into account, leading to a three dimensional problem formulation. The resulting model is shown in Fig. 6. The equations used to compute the resistances and capacities as well as constrains regarding the model are provided in Refs. [24,25].

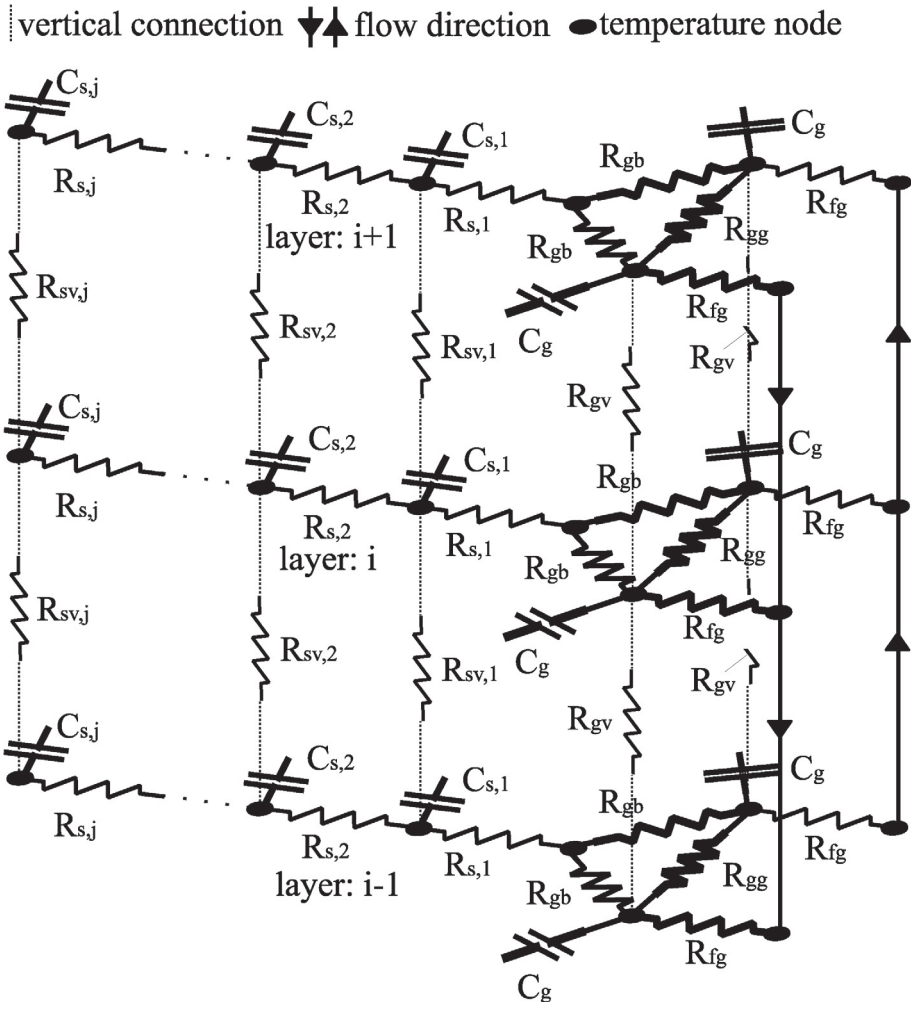

Fig. 6. 3D Model of BHX according to [25].

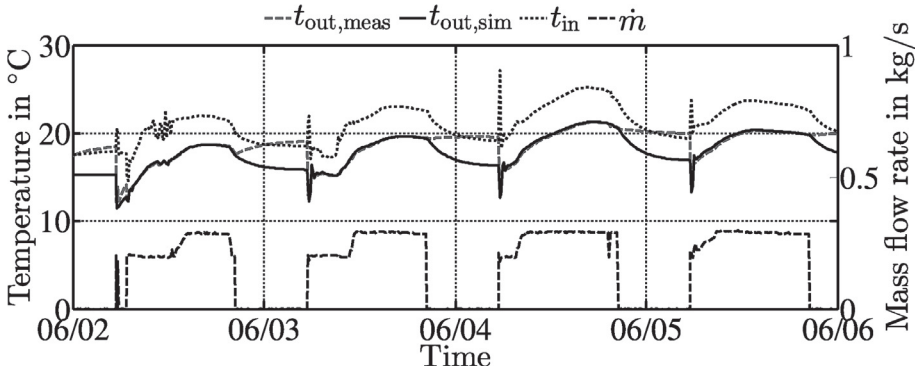

Fig. 7. BHX validation.

Modelica® allows a separate implementation of the defined capacities and resistances which are then connected according to the proposed scheme. The down and upward flowing fluid is modeled as one-dimensional flow discretized using the Finite Volume Method, following the approach presented in Ref. [26]. Two volumes with energy balances are used per layer; one for the downward flowing fluid, one for the upward flowing fluid. The total heat transfer area, volume, and mass flow are the addition of two pipes of the double U-tube heat exchanger. The heat transfer coefficients are calculated based on the velocity in one of the original pipes of the BHX. The transient response of the BHX is governed by the energy balance equation of the fluid volumes and the grout capacities. The fluid volumes are described by equation (1).

$$\frac{dU}{d\tau} = \dot{m}_{in} \cdot h_{in} - \dot{m}_{out} \cdot h_{out} + \dot{Q}_g \tag{1}$$

where $\dot{Q}_g$ is the heat transferred between grout and pipe. The respective balance for the grout and soil thermal masses is given by equation (2).

$$C \frac{dt}{d\tau} = \sum \dot{Q} \tag{2}$$

In order to ensure an efficient and accurate simulation, the choice of the vertical and horizontal discretization parameters is crucial. To determine the horizontal discretization the diameter of the surrounding soil which is influenced by the BHX needs to be determined in the model. According to [27], it is suitable to choose the diameter large enough to ensure that the temperature change of the last soil volume is less than 0.2 °C during a cooling or heating period. In this study, the diameter was calculated to be 15 m. The actual parameters were then determined by modeling one BHX of the test facility and comparing the simulation results to measured data. It was found a finer discretization of the soil next to the borehole is necessary to capture the larger temperature gradient, while the soil farther away can be modeled using bigger volumes. Accordingly, five volumes were used to model the first 3 m surrounding the borehole, the next 3 m were modeled by just one volume and another volume was chosen to model the remaining soil. The vertical discretization was chosen in a way that one layer corresponds to 2 m of soil. Fig. 7 shows a comparison of simulation results and measured data for the BHX outlet temperature. We simulated an entire cooling period and compared it to the measured data in order to validate the model and the chosen parametrization. For better visibility, Fig. 7 only plots four days of data. Data regarding the soil structure next to the BHX as well as tube and borehole geometry are provided in Ref. [18].

The simulated outlet temperature shows a good agreement with the measured outlet temperature as soon as the pump is switched on (visible through the mass flow displayed on the right axis of Fig. 7). Considering the whole cooling period, the averaged absolute error of the outlet temperature is 0.16 °C. Regarding the energy transferred to the soil the error is 2.1%. Therefore, the model is considered suitable for the investigation. Soil data for different locations are hardly available. As conducted in Ref. [14] the same soil property is assumed to surround the BHXs at all locations ($\lambda_S = 1.8\ \mathrm{W\,(mK)^{-1}}, \rho_S = 2100\ \mathrm{kg\,m^{-1}}, c_{p,S} = 1000\ \mathrm{J\,(kgK)^{-1}}$), the same approach is chosen for the grouting material ($\lambda_g = 2\ \mathrm{W\,(mK)^{-1}}, \rho_g = 1460\ \mathrm{kg\,m^{-3}}, c_{p,g} = 1000\ \mathrm{J\,(kgK)^{-1}}$). All other parameters were chosen according to the BHX of the test facility. To define the initial conditions at the beginning of the cooling period, the soil temperature at depth z at the time τ_{start} is estimated using equation (3) [28]:

$$t_{s,initial}(z, t_{Start}) = \bar{t}_a + \Delta t_{a,amp} \cdot \exp(-\xi) \cdot \cos\left(\frac{2\pi \cdot \tau_{Start}}{\tau_0} - \theta_0 - \xi\right) \tag{3}$$

with

$$\xi = z \cdot \sqrt{\frac{\pi \cdot \rho_s \cdot c_{p,s}}{\lambda_s \cdot \tau_0}} \tag{4}$$

After initialization, changes in ambient temperature are considered in the model through vertical conduction under the assumption of ideal heat transfer between air and the surface of the soil.

3.2. Air handling unit

An overview of simplified approaches to model desiccant wheels for system simulation is provided in Ref. [29]. A commonly applied method is the effectiveness method. Two effectiveness parameters are used to describe the global performance of the desiccant wheel. In this study, the enthalpy h as well as the equilibrium water content of the desiccant q are used. Following the definition of [30] the effectiveness parameters are defined according to equation (5):

$$\eta_q = \frac{q_{pro,in} - q_{pro,out}}{q_{pro,in} - q_{reg,out}} \text{ and } \eta_h = \frac{h_{pro,in} - h_{pro,out}}{h_{pro,in} - h_{reg,out}} \tag{5}$$

The equilibrium water content of the desiccant is calculated using the relations provided by Ref. [31]. Unlike other desiccants, lithium chloride does not exhibit continuous isotherms due to the

presence of different phases. For this reason and the explanations provided in Ref. [32], the influence of variable inlet states for process and regeneration air on the effectiveness is taken into account. As rotational speed and both air flow rates are constant in this study, the model does not account for changes regarding these variables. We found that we can predict the outlet conditions of the desiccant wheel by extrapolating the isotherm equations provided by Ref. [31] for the dilute solution and using the effectiveness parameters calculated according to equation (6).

$$\eta_{\boldsymbol{q}} = 1 - \frac{1}{2.32 \cdot \left(q_{\mathrm{pro,in}} - q_{\mathrm{reg,in}}\right) + 3.99} + 0.0006 \cdot q_{\mathrm{pro,in}} \text{ and } \eta_h = 0.14 \tag{6}$$

The desiccant water load is calculated as follows [31].

$$\mathrm{q} = -a(T) \cdot \ln(\varphi)^{\frac{1}{b(T)}} \tag{7}$$

with

$$a(t) = -4 \cdot 10^{-3} \cdot T + 2.2204 \text{ and } b(t) = 4.6 \cdot 10^{-3} \cdot T - 1.3392 \tag{8}$$

We used a detailed and validated model of the desiccant wheel presented in Refs. [33] and [34] in order to calibrate the simplified model. The influence of tested correlations for the parameter η_h on the model accuracy is identified as small, accordingly a constant value is used. The structure of the equation used to calculate η_q was determined based on preliminary analyses. We tested multiple curve functions to fit the simulation results of the detailed model. The present form provided the best calibration results. To find the coefficients (2.32, 3.99 and 0.0006) required to calculate η_q, the detailed model was simulated for a wide range of ambient temperatures and water contents. Furthermore, the regeneration air water content was varied for each ambient condition. Table 2 shows the respective ranges as well as chosen geometric parameters of the desiccant wheel. Excluding outlet conditions which do not satisfy the condition $\varphi < 1$, this procedure leads to 962 test cases. The regeneration air temperature was limited to 70 °C and otherwise controlled to reach a supply air water content of 8.5 g/kg. A comparison between the results obtained by both models regarding supply air outlet temperature and water content is displayed in Fig. 8. Root mean square error regarding the difference in water content is 0.29 g/kg, the respective quantity for the temperature difference is 0.37 °C. The model is therefore considered sufficiently accurate for the conducted study.

The heat recovery wheel, as well as both water-air heat exchangers, are modeled using the well-established $\varepsilon - \mathrm{NTU}$ method [35]. As air and water flows are chosen to be constant the efficiencies of the heat exchangers remain nearly constant for the different operational points. The efficiencies for the water-air heat exchangers $\varepsilon_{\mathrm{WAHX}}$ and the heat recovery wheel $\varepsilon_{\mathrm{HRW}}$ are defined according to equation (9):

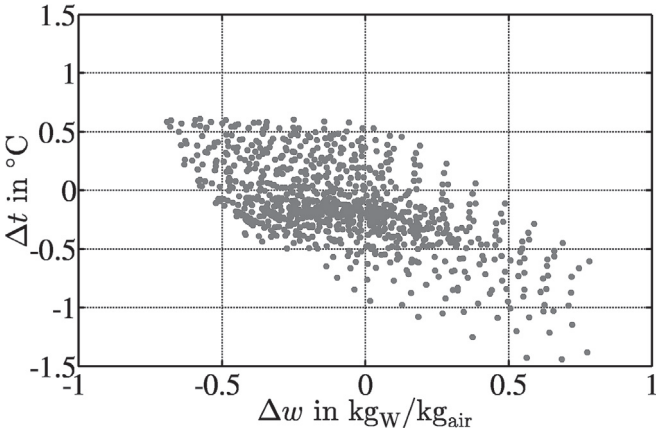

Fig. 8. Comparison between the reference data and the model used in this study.

$$\varepsilon_{\mathrm{WAHX}} = \frac{C_{\mathrm{a}} \cdot \left(t_{\mathrm{a,out}} - t_{\mathrm{a,in}}\right)}{C_{\mathrm{min}} \cdot \left(t_{\mathrm{w,in}} - t_{\mathrm{a,in}}\right)} \text{ and } \varepsilon_{\mathrm{HRW}} = \frac{C_{\mathrm{a,pro}} \cdot \left(t_{\mathrm{a,pro,in}} - t_{\mathrm{a,pro,out}}\right)}{C_{\mathrm{a,min}} \cdot \left(t_{\mathrm{a,pro,in}} - t_{\mathrm{a,reg,in}}\right)} \tag{9}$$

The obtained values are $\varepsilon_{\mathrm{AC}} = 0.66$ for the cooling coil, $\varepsilon_{\mathrm{AH}} = 0.62$ for the heating coil and $\varepsilon_{\mathrm{HRW}} = 0.8$ for the heat recovery wheel. These values are in the range of other efficiencies presented or used in literature [36–39].

3.3. Building model

We used the mixed-air model of the Modelica Buildings library to model the reference room. A validation of the respective model is presented in Ref. [40]. Detailed information regarding the model architecture and the equations used to describe the heat transfer between room and environment are provided in Ref. [41]. The whole room is described by one lumped air control volume. The transient behavior is captured through dynamic energy balances for the respective air and further control volumes for interior, walls, ceiling and the floor. Heat exchange with ambient is computed by solving the heat equation in a one-dimensional formulation using the Finite Volume Method. The number of nodes is chosen as explained in Ref. [42]. To verify the implementation, the obtained results have been compared to results obtained through an EnergyPlus model of the same building. The daily deviations regarding the cooling load are usually smaller than 10%, for the whole month a deviation of 4.9% is obtained. The model is therefore considered suitable for the conducted study.

The cooling ceilings are described using equation (10):

Table 2
Parameters and conditions used for desiccant wheel simulation.

Geometry/Properties		Simulation parameters	range	stepsize
Desiccant material	LiCl	Ambient air temperature	18 °C–35 °C	1 °C
Matrix material	Cellulose	Ambient air water content	10 g/kg – 20 g/kg	1 g/kg
Channel type	Sinusoidal	Regeneration air water content	9 g/kg – 14 g/kg	1 g/kg
Channel height	1.8 mm			
Channel width	3.8 mm			
Rotational speed	16 rph			

$$\dot{Q} = kA \cdot \Delta t_{\ln} \text{ with } \Delta t_{\ln} = \frac{t_{w,in} - t_{w,out}}{\ln \frac{|t_{w,in} - t_{Room}|}{|(t_{w,out} - t_{Room})|}} \quad (10)$$

As described in Ref. [43], the kA value is determined through experimental data. Equation (10) is badly conditioned for $t_{w,in} \approx t_{w,out}$. Therefore, a numerical approximation of the logarithmic mean temperature difference is used for this case as described by Ref. [44]. In a test simulation for a whole cooling period a root mean square error of 69 W is obtained for the transferred heat flow, while the mean value of the heat flow was 1.1 kW during the considered period. We measured the operative temperature as well as the air temperature during the experimental investigations. The occurring differences were usually below 0.1 °C. Accordingly, we considered the air temperature of the simulated reference room as sufficient indicator for thermal comfort.

3.4. Solar thermal system

We used a model of the Modelica Buildings Library to describe the solar thermal collectors. The efficiency for the nominal point is calculated using the Hottel-Whiller-Bliss equation.

$$\eta = \eta_0 - a_1 \cdot \frac{\Delta t_{nom}}{I_{tnom}} - a_2 \cdot \frac{(\Delta t_{nom})^2}{I_{tnom}} \quad (11)$$

The losses occurring in the nominal point ($\Delta t_{nom} = 50\,°C$ and $I_{t_{nom}} = 1000\,W/m^2$) are utilized to define an UA value which leads to the same heat loss at nominal conditions. The respective value is applied to determine losses during simulation. The coefficients η_0, a_1 and a_2 as well as incident angle modifier and thermal collector mass are chosen according to the values provided by Ref. [45] for flat-plate selective collectors. The size of one module is $2.51 m^2$, it is discretized in four segments, each of them containing a transient energy balance. We divided the thermal storage tank into 10 fully mixed volumes of equal size. For each volume a transient energy balance is evaluated. The tank volume is chosen according to the selected collector area A_{SC}:

$$V_T = 100 \frac{l}{m^2} \cdot A_{SC} \quad (12)$$

The tank volume per collector area is chosen twice as big as the rule of thumb provided by Ref. [46]. Our choice is motivated by the absence of auxiliary heating systems and by using preliminary simulation results. All further parameters of the solar system like tank height, insulation and size of the solar heat exchanger were chosen according to [45]. Variable speed pumps are used to feed the solar collectors as well as within the solar tank loop.

3.5. Electricity demand

The electricity demand of the fans and pumps is modeled based on measured data of the test facility in Hamburg. The pumps feeding air cooler, heater, cooling ceilings and BHXs are operated with constant flow rates. Accordingly, a constant electricity demand is assumed. The electricity demand of the variable speed solar pumps is calculated as a function of the relative pump speed f_P using an equation provided by Ref. [47].

$$P_{el}(f_P) = P_{el,nom} \cdot \left(1.31 \cdot f_P^2 + 0.4545 \cdot f_P + 0.137\right) \quad (13)$$

The biggest share of the overall electricity demand is caused by the fans which operate based on the operational mode of the air handling unit. As the volume flow is fixed for supply air conditions, the actual flow through the different components might vary with different operating conditions. The mentioned effect is accounted for by a linear relationship based on the outdoor air temperature. The relationship is fitted by measured data. Table 3 summarizes the electricity demand of the different pumps as well as the aggregated demand of both fans.

3.6. Reference system

In order to evaluate the geothermal cooling within the presented system configuration, sensible cooling through a VCC is modeled as a reference. The BHXs are replaced by a VCC, providing the same cooling power and maintaining the same evaporating temperature as the water temperature. The Carnot efficiency-based model provided by Ref. [48] is used to model the electricity demand of the chiller. The COP is calculated using equation (14).

$$COP = \eta_{C,0} \cdot \frac{T_E}{T_C - T_E} \cdot \eta_{PL} \quad (14)$$

The varying temperature levels at condenser and evaporator are accounted for by the Carnot efficiency. The factor $\eta_{C,0}$ specifies the deviation between the COP and Carnot efficiency at nominal conditions. The COP change under part load conditions is accounted for by the factor η_{PL}. A simple linear degradation is assumed:

$$\eta_{PL} = 1 - c_d\,(1 - PLR) \quad (15)$$

The degradation coefficient is set to $c_d = 0,25$ [49]. The part load ratio PLR is the ratio between actual and nominal cooling capacity. Consumption of the cooling tower fan motor and circulation pumps is assumed to account for 31.4 W for each kW of cooling capacity [49]. The temperatures of evaporator and condenser are assumed to differ by 11.5 °C compared to the respective inlet temperatures; the factor $\eta_{C,0}$ is chosen to be 0.58. The mentioned values have been calibrated using a sample cycle simulated with in-house software VapCyc® [50]. During operating conditions occurring during the conducted simulations, the deviation of COP is less than 5% for all investigated points. A standby consumption of 30 W is assumed.

3.7. Economic evaluation and life cycle climate performance (LCCP)

The BHXs are compared with the reference VCC from an economic and an environmental perspective. The economic assessment is conducted according to [51]. Following this guideline, the life cycle cost of both systems are calculated in form of an annuity A_{LC} which includes three different types of cost:

$$A_{LC} = A_{capital} + A_{operation} + A_{demand} \quad (16)$$

The upfront investment in construction and machinery is covered in the capital related annuity $A_{Capital}$; the operation related annuity $A_{operation}$ takes service and maintenance cost into account. The demand related annuity A_{demand} is calculated based on the electricity consumption of both systems. Main parameters for the economic evaluation are presented in Table 4. Regarding the initial investment for BHXs or vapor compression chillers, varying values are presented in literature. To account for the related uncertainty, minimum and maximum values for the respective quantities are used. Accordingly, a minimum and maximum annuity is presented for each system and location.

We compared the overall environmental impact of both systems, by investigating the LCCP. We determined the lifetime CO_2 emissions of the system by this analysis [57]. For refrigeration systems, the emissions can be grouped into direct and indirect

Table 3
Electricity demand of the different components.

Pump	Electricity demand	Operational mode	Fan electricity demand
P_{CC}, P_{AC}, P_{AH}	20 W	OM 1	330 W
P_{BHX}	35 W	OM 2	$f(t_{out})$, 610 W-690 W
P_{SC}, P_{TL}	$f(f_P^2, f_P, P_{nom})$	OM 3,4	$f(t_{out})$, 410 W-430 W

Table 4
Parameters for economic evaluation.

Parameter	Value	Cost	Value
General		*Investment cost*	
Observation period	20 years [6,7]	BHX	40 - 72 $/m [54]
Interest rate	4% [52]	VCC	200 - 415 $/kW [6,55]
Price change factors		Glycol	6.36 $/kg [53]
Energy	2%	*Maintenance cost*	
Maintenance	2%	BHX	50 $/year (Annuity)
Investment	2%	VCC	100 $/year (Annuity)
Lifespan		*Electricity prices* [56]	
BHX	50 years [51]	Chicago	9.4 ct./kWh
VCC	15 years [51]	New York	15.3 ct./kWh
Glycol	10 years [53]	Washington	12.1 ct./kWh
		San Diego	15.4 ct./kWh
		San Francisco	15.4 ct./kWh

emissions. Direct emissions account for refrigerant leakage over the lifetime of the system. Indirect emissions are caused by the use of the system over its lifetime. They account for emissions from electricity generation, as well as manufacturing and disposal of the different components. Detailed information to calculate the different terms can be found in Ref. [58]. Regarding the BHX the emissions due to construction such as the fuel consumption to drill the boreholes or transportation of the displaced soil need to be accounted for besides the emissions for manufacturing and disposal of the components and the respective electricity consumption of the pumps. Explanations regarding the different materials and processes can be found in Ref. [59]. Table 5 contains the most important parameters for the LCCP analysis. As the lifespan for the BHXs is more than three times longer than the lifespan of the VCC (see Table 4), the aggregated emissions for VCC are multiplied by the ratio of these values to obtain comparable data.

4. Simulation results and discussion

The system configurations for the different locations are displayed in Table 6. Besides solar collector area and number and depth of the BHXs boundary conditions, such as the yearly average ambient temperature and the occurring sensible and latent loads are presented. The respective loads are evaluated for the whole period p and calculated according to equation (17).

$$Q_{lat} = \int_p \dot{m}_{sup} \cdot (h_1 - h(t_1, w_4)) d\tau \text{ and } Q_{sen} = \int_p \left[\dot{m}_{sup} \cdot (h_1 - h(t_4, w_1)) + \dot{m}_{w,\ CC} \cdot (h_{out} - h_{in})\right]\ d\tau \quad (17)$$

The last three columns mark the remaining percentage of uncomfortable room states; t_{vl} and w_{vl} describe the ratio of room air states which violate the comfort criterions regarding temperature and humidity. The last column gives the overall percentage of uncomfortable room states. The size of the solar thermal system is mainly related to the latent loads. However, solar availability as well as ambient temperatures which impact the desiccant wheel performance also influence the respective size. The size of the geothermal system is mainly influenced by the temperature of the undisturbed soil, indicated by the yearly average temperature and the sensible load. The strong influence of the soil temperature can be discerned from comparing the size of the BHXs for Chicago and San Diego. While the sensible cooling demand during the investigated period is 1.6 times higher for Chicago, the overall size of the geothermal system is 2.5 times larger for San Diego. Considering the presented shares of uncomfortable room states, it is easy to see

Table 6
System parameters and climatic boundary conditions.

	$\varnothing t_{a,0}$	Q_{sen}	Q_{lat}	A_{SC}	h_{BHX}	n_{BHX}	t_{vl}	w_{vl}	overall
	(°C)	kWh	kWh	m²	m	–	%	%	%
Chicago	10.0	3374	3219	17.6	60	2	4.0	4.6	6.8
New York	12.5	3637	3876	22.6	100	2	3.4	3.3	5.3
Washington	14.1	4789	4583	27.6	90	4	4.4	4.9	7.4
San Diego	17.7	2115	3426	10.0	100	3	4.5	0.9	5.1
San Francisco	13.0	1087	337	2.5	40	1	4.3	0.3	4.4

Table 5
Parameters for life cycle climate performance.

Parameter BHX	Value	Parameter VCC	Value
Manufacturing/disposal		*Refrigerant leakage*	
Polyethylene	2.54 kgCO_{2e}/kg [60]	Refrigerant	R410 A
Bentonite	70 kgCO_{2e}/t [59]	Charge	0.3 kg/kW [62]
Glycol	3.02 kgCO_{2e}/l [61]	Annual leakage rate	6% [62]
Construction		Service leakage	5% [57]
Drilling	2.68 l diesel/m [62]	End of life leakage	10% [57]
Disposal of soil	6.66 l diesel/t (calculated based on [59])	GWP R410A	2088 kg CO_{2e}/kg
Diesel	2,68 kgCO_{2e}/l [63]	*Manufacturing/disposal*	
Electricity demand		Weight	10 kg/kW
Western Interconnection	0.594 kg CO_2/kWh	Material	Steel (46%): 1.9 kg CO_{2e}/kg, Aluminium (12%): 12.7 kg CO_{2e}/kg, Copper (19%): 3.1 kg CO_{2e}/kg, Plastic (23%): 2.8 kg CO_{2e}/kg, R410A 10.7 CO_{2e}/kg
Eastern Interconnection	0.788 kg CO_2/kWh	*Electricity demand*	
		Western Interconnection	0.594 kg CO_2/kWh
		Eastern Interconnection	0.788 kg CO_2/kWh

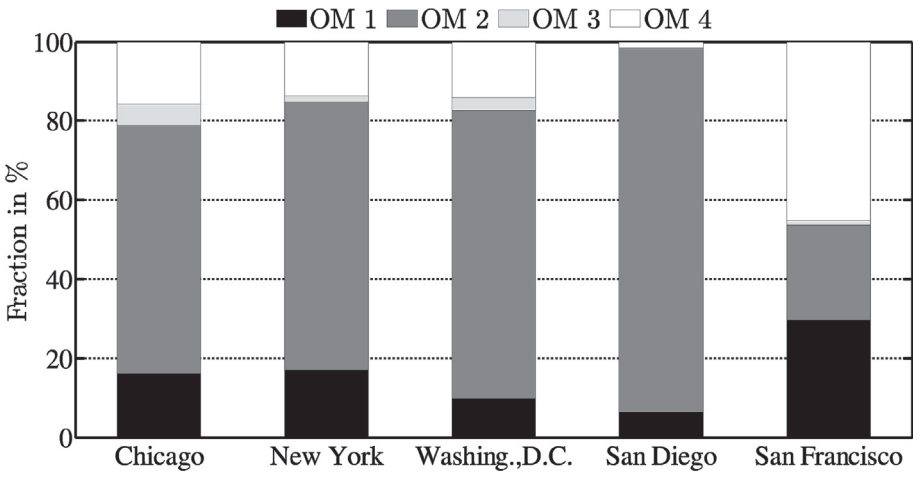

Fig. 9. Share of the operational modes.

that the system is capable of delivering sufficient air conditioning (t_{vl} and w_{vl} both below 5%) at all considered locations.

The share of the different OMs regarding the air handling unit is displayed in Fig. 9. The cooling and dehumidification mode (OM2) exhibits the overall highest share with an average of 64% for all locations. The highest share of the pure ventilation mode (OM1) occurs in San Francisco with nearly 30%, while the mode accounts for less than 6% in San Diego. Bypasses are activated for 36% of the operating time, averaged over all locations.

4.1. Room air temperature and humidity

Exemplary results regarding the room air states are displayed in Fig. 10 for New York. The graphs contain daily minimum and maximum values of ambient and room air water content and temperature. The ambient air states are evaluated during night and daytime, while the room air states are just evaluated during the occupation time.

Regarding the water content, the limit of 12 g/kg cannot be maintained during 16 days of the considered period. Of the 16 days, eight days exhibit a maximum water content of more than 13 g/kg and three days exceeded 14 g/kg. The deviations are caused by both too low thermal storage tank temperatures and the dehumidification capacity of the desiccant wheel. The highest room air water content occur on August 17th. On this day, the maximum regeneration air temperature of 70 °C can be maintained during the whole day. However, due to the high ambient air water content of 20.9 g/kg the room air cannot be maintained below the given limit during the whole occupation time. The limits of desiccant dehumidification need to be considered when applying the proposed system for Washington, D.C., Chicago and New York. Pre-cooling and dehumidification is a possible solution to account for those conditions. Given the high dew point temperature, this could possibly be achieved by BHXs. In general, the system is able to remove a high fraction of the latent loads during the whole cooling period.

During our investigation the room temperature exceeds the chosen limit of 27 °C during 14 days, however only four days exhibit maximum temperatures above 28 °C. For days with a maximum ambient temperature below 31 °C the room temperature can generally be kept within the comfort region. However, one can see that besides the actual loads the point of time within the cooling period plays a key role in regards to the cooling ability of the system, as the soil temperature varies throughout this period. The highest ambient temperatures of 35 °C occur on May 28th and 29th, and the room maintains a temperature below 28 °C during both days. The highest room temperature of 29 °C is obtained on August 17th, coinciding with a maximum ambient temperature of 32 °C. As visible in Fig. 10, over several days the minimum room temperature is below 22 °C. As we did not simulate an active heating device for this study, we did not include the respective points in the thermal comfort evaluation.

We conducted a parametric study regarding the size of the geothermal system in New York to provide deeper insights into seasonal and short-term warming of the soil and the respective influence on thermal comfort. The depth of the two BHXs is varied

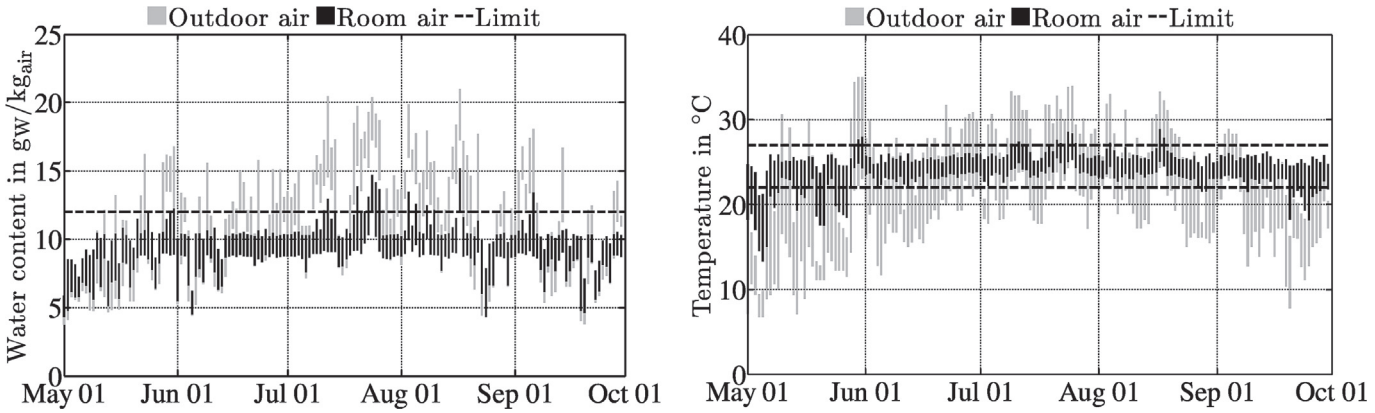

Fig. 10. Ambient and room air states during the investigated period for New York.

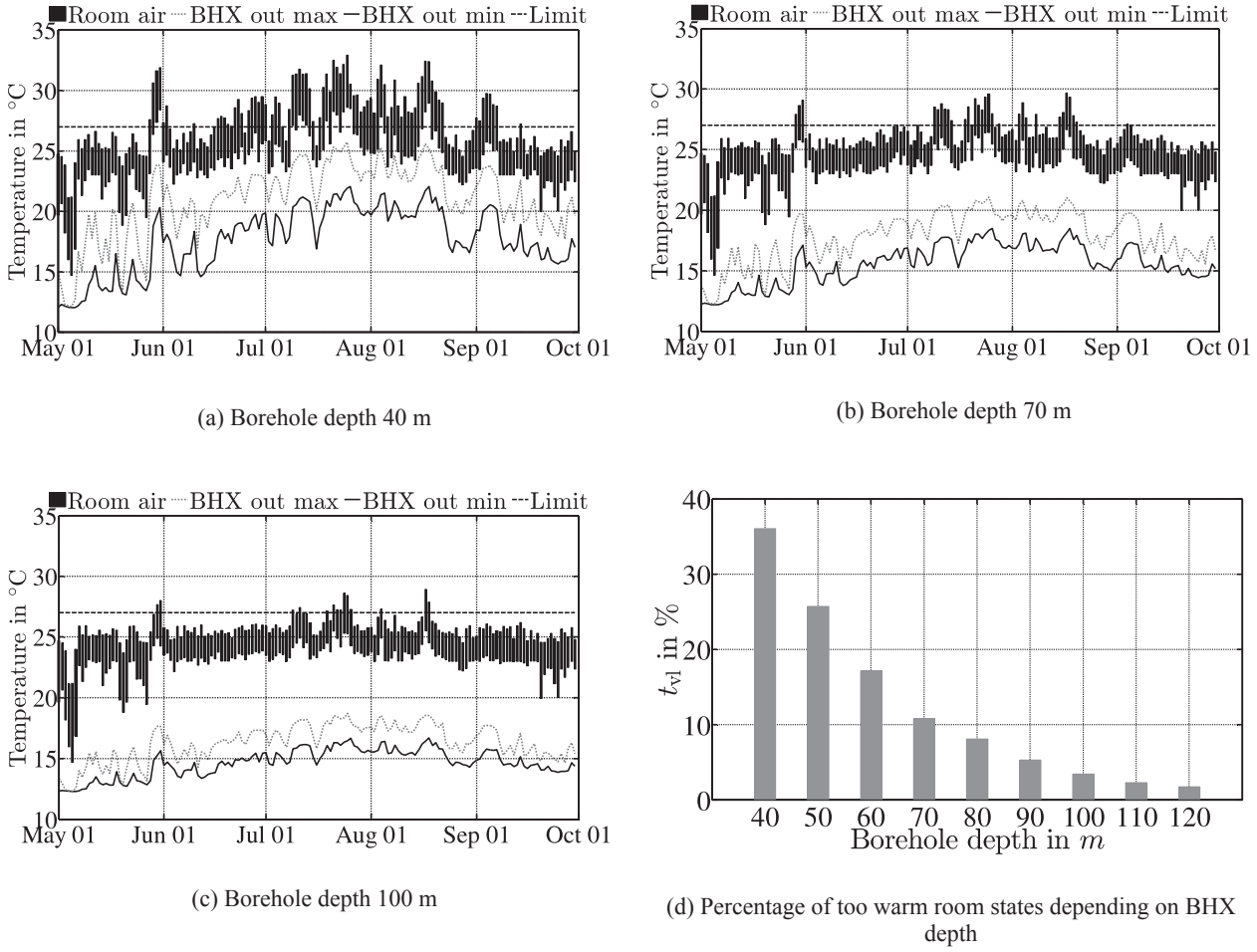

(a) Borehole depth 40 m

(b) Borehole depth 70 m

(c) Borehole depth 100 m

(d) Percentage of too warm room states depending on BHX depth

Fig. 11. Influence of borehole depth on thermal comfort for New York.

between 40 m and 120 m. Fig. 11 shows simulation results for borehole depths of 40 m, 70 m, and 100 m by comparing minimum and maximum room air and BHX outlet temperatures. Fig. 11(d) shows the corresponding percentage of uncomfortable hot room states during the cooling period for different borehole depths. Seasonal and short-term fluctuations of the BHX outlet temperatures are reduced with increasing borehole length. The minimum outlet temperatures occur at the beginning of the cooling period and are similar for all three configurations (around 12.5 °C). The maximum outlet temperatures are reached in July and August. Temperatures below 26 °C, 21 °C, and 19 °C are maintained by the different configurations throughout the cooling period. For a depth of 40 m, the room temperature exceeds 30 °C during 26 days, while this threshold is not reached during a single day for borehole depths of 70 m or 100 m. For deeper boreholes, the additional gain in thermal comfort per additional depth decreases. The allowed percentage of uncomfortable room states is a critical parameter during the sizing of the proposed system; the tradeoff between borehole depth, which is usually directly related to investment cost, and thermal comfort is particularly important.

4.2. Energetic performance

The efficiency of the proposed system is evaluated regarding its latent, thermal and electric efficiency ratios (e.g. Refs. [64,65]). They are defined according to equation (18).

$$\mathrm{SER}_{\mathrm{lat}} = \frac{Q_{\mathrm{lat}}}{\int_{\mathrm{OM2}} \dot{m}_{\mathrm{w,AH}} \cdot (h_{\mathrm{in}} - h_{\mathrm{out}})\ \mathrm{d}\tau} \quad \mathrm{SER}_{\mathrm{th}} = \frac{\int_{\mathrm{OM2}} [\dot{m}_{\mathrm{sup}} \cdot (h_1 - h_4) + \dot{m}_{\mathrm{w,\ CC}} \cdot (h_{\mathrm{out}} - h_{\mathrm{in}})]\mathrm{d}\tau}{\int_{\mathrm{OM2}} \dot{m}_{\mathrm{w,AH}} \cdot (h_{\mathrm{in}} - h_{\mathrm{out}})\ \mathrm{d}\tau}$$

$$\mathrm{SER}_{\mathrm{el}} = \frac{\int_{\mathrm{OM2}} [\dot{m}_{\mathrm{sup}} \cdot (h_1 - h_4) + \dot{m}_{\mathrm{w,\ CC}} \cdot (h_{\mathrm{out}} - h_{\mathrm{in}})]\mathrm{d}\tau}{\int_{\mathrm{OM2}} P_{\mathrm{el}}\ \mathrm{d}\tau} \tag{18}$$

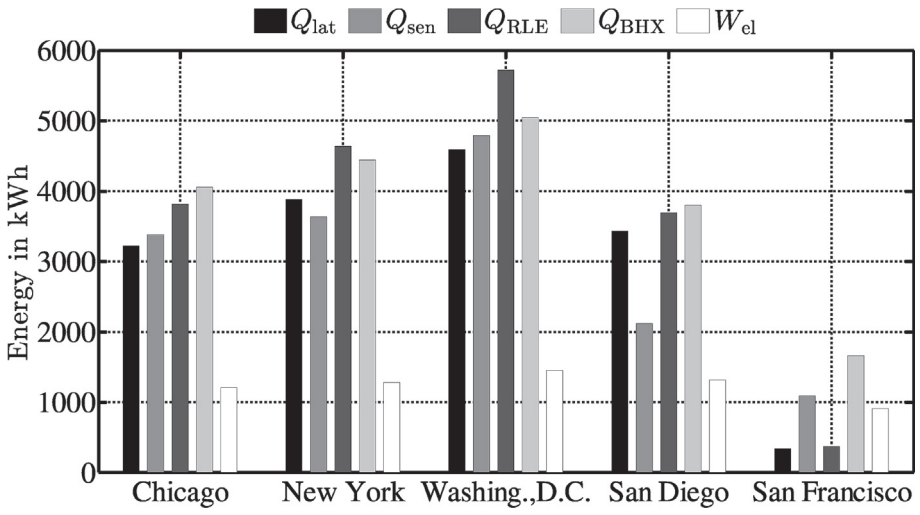

Fig. 12. Loads and energy demands for the different locations.

Table 7
Seasonal Efficiency Ratios for the evaluated system.

	SER_{lat}	SER_{th}	SER_{el}
Chicago	0.85	1.55	6.89
New York	0.84	1.49	7.20
Washington	0.80	1.52	7.66
San Diego	0.93	1.40	4.18
San Francisco	0.93	1.24	1.55

SER_{lat} is the ratio of the latent load removed by the air handling unit and the energy required for regeneration of the desiccant. The thermal efficiency SER_{th} relates the overall cooling provision to the energy required for regeneration. The electric efficiency SER_{el} is derived by dividing the provided cooling energy by the overall electricity demand of the system. The respective quantities are evaluated solely for the second operational mode. Fig. 12 shows the sensible and latent loads handled by the air conditioning system, the energy transferred in the regeneration air heater, the boreholes as well as the electricity demand of the system. Table 7 shows the above-defined SERs for the chosen locations.

The energy demand for regeneration is closely related to the latent loads. The varying differences between both quantities among locations are caused by different ambient temperatures. Lower temperatures are more favorable for desiccant dehumidification. Accordingly, the latent SER exhibits higher values for San Diego and San Francisco, where the latent loads usually occur at lower ambient temperatures. The energy transferred through the BHX is primarily depending on the occurring sensible loads. However, the energy transferred through the soil exceeds the sensible load for all locations. This is partly due to the limited efficiency of the heat recovery wheel and partly due to temperature levels of ambient air and room air. If latent loads occur at temperature levels between room and supply air temperature or even below supply air temperature, the temperature level behind the heat recovery wheel (position 3 in Fig. 1) is still limited by the room air temperature. The second reason causes the comparatively large difference between both quantities for San Diego. Accordingly, a complete separation of latent and sensible cooling cannot be achieved by the presented hybrid system. The electricity demand of the system varies between 899 kWh for San Francisco and 1444 kWh for Washington, D.C. The changes are caused by the

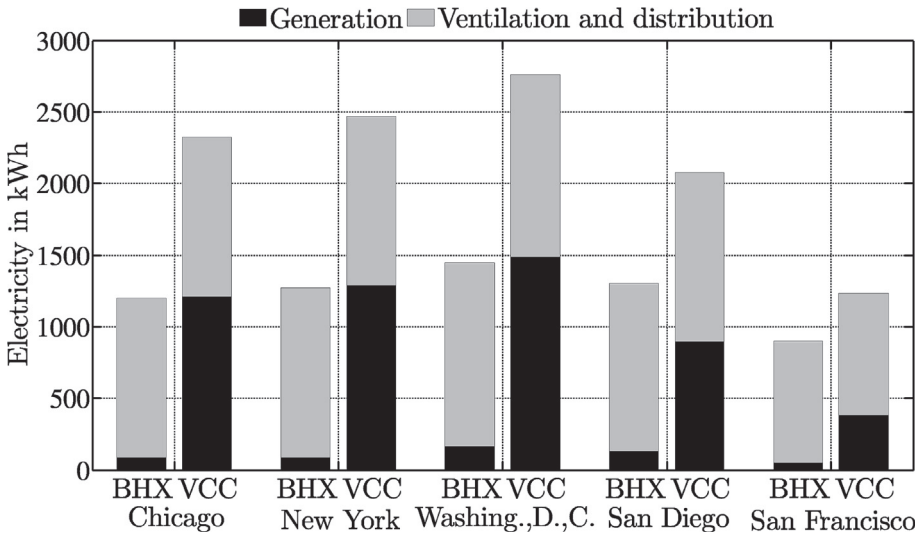

Fig. 13. Electricity demand of the proposed (BHX) and the reference (VCC) system.

Table 8
SERs calculated for the chiller of the reference system.

	Chicago	New York	Washington,D.C.	San Diego	San Francisco
SER_{Ch}	3.29	3.41	3.36	4.22	4.24
$\dot{Q}_{Ch}$	6 kW	6 kW	6 kW	4 kW	2 kW

different OMs of the air handling unit as well as the pump electricity demand for the different configurations. The highest value of $SER_{el} = 7.66$ is achieved in Washington D.C., according to the highest loads occurring in this location. The thermal efficiencies all exceed unity, marking an efficient system operation.

4.3. Comparison with reference system

The electricity demand of the proposed system compared to the reference system is displayed in Fig. 13. The gray part of the bars indicates the amount required for ventilation and distribution while the black part marks the electricity demand to run the chiller or the pumps of the BHXs.

About 50% of the electricity required to run the reference system can be saved by the investigated system in Chicago, New York and Washington, D.C. For San Diego and San Francisco savings are of 37% and 27%. While the electricity demand of the BHX pumps accounts for an average of 8% of the electricity required to run the investigated system, the chiller is responsible for 46% of the electricity demand in the reference system. The lower demand for San Diego and San Francisco is not solely caused by lower cooling loads; the chiller efficiency is higher at these locations owing to the lower ambient temperatures. The calculated Seasonal Efficiency Ratios ($SER_{Ch} = Q_{Ch}/W_{ch,el}$) for the chiller are provided in Table 8 for reproducibility. Furthermore, chiller capacities are provided, as they are a required input for the economic and the LCCP analyses.

Results regarding the economic comparison between both systems at various locations are presented in Fig. 14. For each location

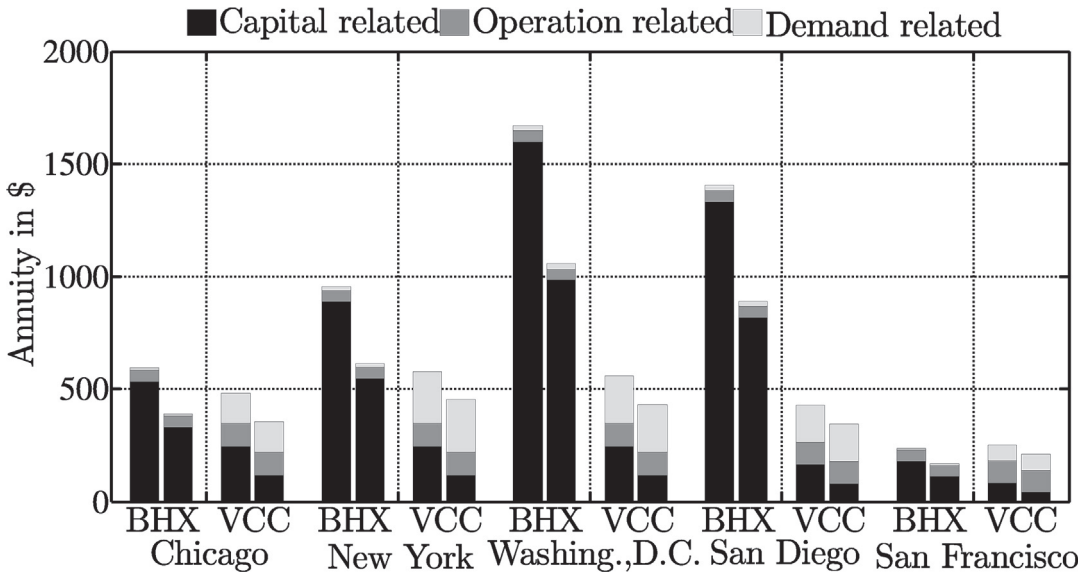

Fig. 14. Minimum and maximum annuities for the BHXs and VCCs at the different locations.

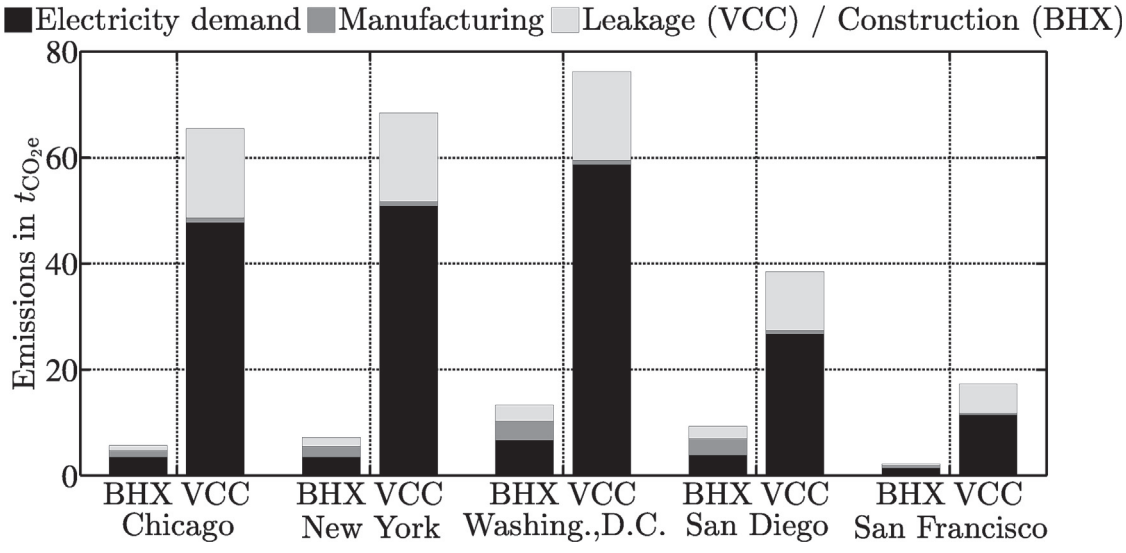

Fig. 15. Total equivalent CO_2 emissions.

minimum and maximum annuities using low and high investment cost (see Table 3) are provided for each configuration. BHXs can be cost-competitive in Chicago and San Francisco, depending on the actual investment necessary set up the BHXs or the VCC. For Washington, D.C. and San Diego the maximum annuity of the BHXs exceeds the maximum one for the VCC by a factor of 3 or 3.3, respectively. At these locations, the necessary size of the geothermal system caused by the comparatively high soil temperatures leads to high upfront investment cost. In general the annuity of the BHXs mainly influenced by the capital related part, which accounts for more than 80% of the minimum and maximum annuities for Chicago, New York, Washington and San Diego; the demand related parts account for less than 5% among these locations.

The comparison of both configurations regarding their LCCP is displayed in Fig. 15. It is visible that considerable CO_{2e} savings are possible through the usage of BHXs in the presented system configuration. The emissions through refrigerant leakage in VCC alone outnumber the overall emissions of BHXs for all locations. The largest share of the emissions related to the VCCs is caused by their electricity demand, which ranges between 66% and 77% for the different locations. While component manufacturing is not significant for the emissions caused by VCCs, the share is higher for the BHXs, where it accounts for up to 33% of the total emissions. The main fraction of this amount is related to the manufacturing of glycol, which is replaced in a ten-year cycle. Due to the long lifespan of the BHXs, the emissions due to construction account for the lowest share while the highest share among all locations is caused by the electricity demand (between 41% and 66%). Overall, the emission reduction through the replacement of a VCC by a geothermal heat sink varies between 76% and 91%.

5. Conclusions

The combination of desiccant dehumidification and sensible cooling with borehole heat exchangers can deliver comfortable indoor conditions at various locations. The size of the geothermal part depends strongly on the undisturbed soil temperature and the sensible loads. The electricity demand of the system is reduced to the required amount to run fans and pumps and considerable savings compared to conventional reference systems are achieved. Depending on the latent and sensible loads, the proposed system achieves Seasonal Efficiency Ratios for cooling and dehumidification of up to 7.66. Contingent upon the necessary depth and number of the borehole heat exchangers required for each location, they can be cost competitive compared to a vapor compression cycle for Chicago and San Francisco. For Washington, D.C. and San Diego their annuities are more than three times higher. The Life Cycle Cost Performance of the borehole heat exchangers exceeds the vapor compression cycle for all investigated locations; emission savings between 91% and 71% can be realized by including shallow geothermal energy.

Acknowledgement

This work is being conducted in the frame of a project funded by the German Federal Ministry for Economic Affairs and Energy (www.bmwi.de), cf. project funding reference number 03ET1065A. The support from Modeling and Optimization consortium in Center for Environmental Energy Engineering, University of Maryland is also greatly appreciated.

References

[1] Davis LW, Gertler PJ. Contribution of air conditioning adoption to future energy use under global warming. Proc Natl Acad Sci U. S. A 2015;112:5962–7. https://doi.org/10.1073/pnas.1423558112.
[2] Isaac M, van Vuuren DP. Modeling global residential sector energy demand for heating and air conditioning in the context of climate change. Energy Pol 2009;37:507–21. https://doi.org/10.1016/j.enpol.2008.09.051.
[3] US department of energy. Residential energy consumption survey. 2015.
[4] Angrisani G, Capozzoli A, Minichiello F, Roselli C, Sasso M. Desiccant wheel regenerated by thermal energy from a microcogenerator: experimental assessment of the performances. Appl Energy 2011;88:1354–65. https://doi.org/10.1016/j.apenergy.2010.09.025.
[5] Khalid A, Mahmood M, Asif M, Muneer T. Solar assisted, pre-cooled hybrid desiccant cooling system for Pakistan. Renew Energy 2009;34:151–7. https://doi.org/10.1016/j.renene.2008.02.031.
[6] Wrobel J, Sanabria Walter P, Schmitz G. Performance of a solar assisted air conditioning system at different locations. Sol Energy 2013;92:69–83. https://doi.org/10.1016/j.solener.2013.02.030.
[7] Angrisani G, Diglio G, Sasso M, Calise F. Dentice d'Accadia M. Design of a novel geothermal heating and cooling system: energy and economic analysis. Energy Convers Manag 2016;108:144–59. https://doi.org/10.1016/j.enconman.2015.11.001.
[8] Casas W, Schmitz G. Experiences with a gas driven, desiccant assisted air conditioning system with geothermal energy for an office building. Energy Build 2005;37:493–501. https://doi.org/10.1016/j.enbuild.2004.09.011.
[9] Angrisani G, Minichiello F, Roselli C, Sasso M. Experimental investigation to optimise a desiccant HVAC system coupled to a small size cogenerator. Appl Therm Eng 2011;31:506–12. https://doi.org/10.1016/j.applthermaleng.2010.10.006.
[10] Beccali M, Finocchiaro P, Nocke B. Energy performance evaluation of a demo solar desiccant cooling system with heat recovery for the regeneration of the adsorption material. Renew Energy 2011;44:40–52. https://doi.org/10.1016/j.renene.2011.12.021.
[11] Ling J, Kuwabara O, Hwang Y, Radermacher R. Experimental evaluation and performance enhancement prediction of desiccant assisted separate sensible and latent cooling air-conditioning system. Int J Refrig 2011;34:946–57. https://doi.org/10.1016/j.ijrefrig.2010.12.008.
[12] Speerforck A, Schmitz G. Integration of an adsorption chiller in an open-cycle desiccant-assisted air-conditioning system. Sci Technol Built Environ 2015:21. https://doi.org/10.1080/23744731.2015.1015382.
[13] Fong KF, Chow TT, Lee CK, Lin Z, Chan LS. Comparative study of different solar cooling systems for buildings in subtropical city. Sol Energy 2010;84:227–44.
[14] Eicker U, Vorschulze C. Potential of geothermal heat exchangers for office building climatisation. Renew Energy 2009;34:1126–33. https://doi.org/10.1016/j.renene.2008.06.019.
[15] Kaushal M. Geothermal cooling/heating using ground heat exchanger for various experimental and analytical studies: comprehensive review. Energy Build 2017;139:634–52. https://doi.org/10.1016/j.enbuild.2017.01.024.
[16] Enteria N, Yoshino H, Takaki R, Mochida A, Satake A, Baba S, et al. Case analysis of utilizing alternative energy sources and technologies for the single family detached house. Sol Energy 2014;105:243–63. https://doi.org/10.1016/j.solener.2014.03.005.
[17] El-Agouz SA, Kabeel AE. Performance of desiccant air conditioning system with geothermal energy under different climatic conditions. Energy Convers Manag 2014;88:464–75. https://doi.org/10.1016/j.enconman.2014.08.027.
[18] Speerforck A, Schmitz G. Experimental investigation of a ground-coupled desiccant assisted air conditioning system. Appl Energy 2016;181:575–85. https://doi.org/10.1016/j.apenergy.2016.08.036.
[19] Modelica Association. Modelica® - a unified object-oriented language for systems modeling language specification version 3.3 revision 1. 2014.
[20] Wrobel J. Entwicklung und bewertung eines konzeptes zur sorptionsgestützten klimatisierung von gebäuden. Hamburg University of Technology; 2014.
[21] ASHRAE. Thermal environmental conditions for human occupancy 55-2010. 2012.
[22] Calise F, Dentice d'Accadia M, Roselli C, Sasso M, Tariello F. Desiccant-based AHU interacting with a CPVT collector: simulation of energy and environmental performance. Sol Energy 2014;103:574–94. https://doi.org/10.1016/j.solener.2013.11.001.
[23] DIN EN 15251. Eingangsparameter für das raumklima zur auslegung und bewertung der energieeffizienz von gebäuden. 2007.
[24] Bauer D, Heidemann W, Müller-Steinhagen H, Diersch HJG. Thermal resistance and capacity models for borehole heat exchangers. Int J Energy Res 2011;35:312–20. https://doi.org/10.1002/er.1689.
[25] Bauer D, Heidemann W, Diersch HJG. Transient 3D analysis of borehole heat exchanger modeling. Geothermics 2011;40:250–60. https://doi.org/10.1016/j.geothermics.2011.08.001.
[26] Pfafferott T, Schmitz G. Modelling and transient simulation of CO2-refrigeration systems with Modelica. Int J Refrig 2004;27:42–52. https://doi.org/10.1016/S0140-7007(03)00098-7.
[27] Bauer D. Zur thermischen modellierung von erdwärmesonden und erdsonden-wärmespeichern. Universitat Stuttgart; 2011.
[28] Ramming K. Bewertung und optimierung oberflächennaher

Erdwärmekollektoren für verschiedene lastfälle. Technischen Universität Dresden; 2007.
[29] Enteria N, Hazim A, Yoshino H, editors. Desiccant heating, ventilating, and air-conditioning systems; 2017. https://doi.org/10.1007/978-981-10-3047-5.
[30] Ruivo CR, Carrillo-Andrés A, Costa JJ, Domínguez-Muñoz F. Exponential correlations to predict the dependence of effectiveness parameters of a desiccant wheel on the airflow rates and on the rotation speed. Appl Therm Eng 2013;51:442–50. https://doi.org/10.1016/j.applthermaleng.2012.08.037.
[31] Casas W. Untersuchung und optimierung sorptionsgestützter Klimatisierungsprozesse. TU Hamburg-Harburg; 2005.
[32] Ruivo CR, Fernández Hernández F, Cejudo López JM. Influence of the desiccant wheel effectiveness method approaches, with fix and variable effectiveness parameters, on the performance results of an airport air-conditioning system. Energy Convers Manag 2015;94:458–71. https://doi.org/10.1016/j.enconman.2015.01.090.
[33] Wrobel J, Morgenstern P, Schmitz G. Modeling and experimental validation of the desiccant wheel in a hybrid desiccant air conditioning system. Appl Therm Eng 2013;51:1082–91. https://doi.org/10.1016/j.applthermaleng.2012.09.033.
[34] Casas W, Prölß K, Schmitz G. In: Modeling of desiccant assisted air conditioning systems. 4th Int Model Conf; 2005. p. 487–96.
[35] VDI. VDI-Wärmeatlas, 11. Auflage. 2013. https://doi.org/10.1007/978-3-642-19981-3.
[36] Panaras G, Mathioulakis E, Belessiotis V, Kyriakis N. Theoretical and experimental investigation of the performance of a desiccant air-conditioning system. Renew Energy 2010;35:1368–75. https://doi.org/10.1016/j.renene.2009.11.011.
[37] Angrisani G, Roselli C, Sasso M. Experimental validation of constant efficiency models for the subsystems of an unconventional desiccant-based Air Handling Unit and investigation of its performance. Appl Therm Eng 2012;33–34:100–8. https://doi.org/10.1016/j.applthermaleng.2011.09.018.
[38] Bourdoukan P, Wurtz E, Joubert P. Comparison between the conventional and recirculation modes in desiccant cooling cycles and deriving critical efficiencies of components. Energy 2010;35:1057–67. https://doi.org/10.1016/j.energy.2009.06.021.
[39] Hürdoğan E, Büyükalaca O, Yılmaz T, Hepbaşlı A. Experimental investigation of a novel desiccant cooling system. Energy Build 2010;42:2049–60. https://doi.org/10.1016/j.enbuild.2010.06.014.
[40] Nouidui TS, Phalak K, Zuo W, Wetter M. In: Validation and application of the room model of the Modelica buildings library. Proc. 9th int. Model. Conf. Munich, ger; 2012. p. 727–36. https://doi.org/10.3384/ecp12076727.
[41] Wetter M, Zuo W, Nouidui TS. Modeling of heat transfer in rooms in the Modelica "Buildings " library. Proc Build Simul 2011;2011:14–6.
[42] Wetter M. Simulation-based building energy optimization. Berkeley: University of California; 2004. https://doi.org/10.1017/CBO9781107415324.004.
[43] Fonseca Diaz N, Lebrun J, André P. Experimental study and modeling of cooling ceiling systems using steady-state analysis. Int J Refrig 2010;33:793–805. https://doi.org/10.1016/j.ijrefrig.2009.12.011.
[44] Mattsson S. On modelling of heat exchangers in modelica. ESS'97-European Simul Symp. 1997. p. 1–7.
[45] Heimrath R, Haller M. The reference heating system, the template solar system of task 32. IEA SHC - task 32-adv storage concepts sol low energy build. 2007. p. 47.
[46] Henning HM, Motta M, Mugnier D. Solar cooling handbook: a guide to solar assisted cooling and dehumidification processes. Ambra Verlag; 2013.
[47] Nienborg B, Dalibard A, Schnabel L, Eicker U. Approaches for the optimized control of solar thermally driven cooling systems. Appl Energy 2017;185:732–44. https://doi.org/10.1016/j.apenergy.2016.10.106.
[48] Wetter M. In: Modelica library for building heating, ventilation and air-conditioning systems. 7th model. Conf; 2009. p. 10. https://doi.org/10.3384/ecp09430042.
[49] AHRI. Standard. Performance rating of unitary air-conditioning & air-source heat pump equipment. ANSI/AHRI stand 210/240, vol. 2; 2008. p. 136.
[50] Winkler J, Aute V, Radermacher R. Comprehensive investigation of numerical methods in simulating a steady-state vapor compression system. Int J Refrig 2008;31:930–42. https://doi.org/10.1016/j.ijrefrig.2007.08.008.
[51] VDI. VDI 2067-Fundamentals and economic calculation. 2012.
[52] Larranaga MD, Beruvides MG, Holder HW, Karnuasena E. Strauss DC. DOAS & humidity control. ASHRAE J 2008:1.
[53] Emmi G, Zarrella A, De Carli M, Donà M, Galgaro A. Energy performance and cost analysis of some borehole heat exchanger configurations with different heat-carrier fluids in mild climates. Geothermics 2017;65:158–69. https://doi.org/10.1016/j.geothermics.2016.09.006.
[54] Junghans L. Evaluation of the economic and environmental feasibility of heat pump systems in residential buildings, with varying qualities of the building envelope. Renew Energy 2015;76:699–705. https://doi.org/10.1016/j.renene.2014.11.037.
[55] Al-Alili A, Islam MD, Kubo I, Hwang Y, Radermacher R. Modeling of a solar powered absorption cycle for Abu Dhabi. Appl Energy 2012;93:160–7. https://doi.org/10.1016/j.apenergy.2010.11.034.
[56] U.S. Energy information administration. State electricity profiles. 2017. https://www.eia.gov/electricity/state/.
[57] Beshr M, Aute V, Sharma V, Abdelaziz O, Fricke B, Radermacher R. A comparative study on the environmental impact of supermarket refrigeration systems using low GWP refrigerants. Int J Refrig 2015;56:154–64. https://doi.org/10.1016/j.ijrefrig.2015.03.025.
[58] Beshr M, Aute VC. LCCP desktop application v1.0 engineering reference. 2013.
[59] Genchi Y, Kikegawa Y, Inaba A. CO2 payback-time assessment of a regional-scale heating and cooling system using a ground source heat-pump in a high energy-consumption area in Tokyo. Appl Energy 2002;71:147–60. https://doi.org/10.1016/S0306-2619(02)00010-7.
[60] Moran P, Goggins J, Hajdukiewicz M. Super-insulate or use renewable Technology? Life cycle cost, energy and global warming potential analysis of nearly zero energy buildings (NZEB) in a temperate oceanic climate. Energy Build 2017;139:590–607. https://doi.org/10.1016/j.enbuild.2017.01.029.
[61] Beccali M, Cellura M, Longo S, Mugnier D. A simplified LCA tool for solar heating and cooling systems. Energy Procedia 2016;91:317–24. https://doi.org/10.1016/j.egypro.2016.06.226.
[62] Saner D, Juraske R, Kübert M, Blum P, Hellweg S, Bayer P. Is it only CO2 that matters? A life cycle perspective on shallow geothermal systems. Renew Sustain Energy Rev 2010;14:1798–813. https://doi.org/10.1016/j.rser.2010.04.002.
[63] Turner LK, Collins FG. Carbon dioxide equivalent (CO2-e) emissions: a comparison between geopolymer and OPC cement concrete. Constr Build Mater 2013;43:125–30. https://doi.org/10.1016/j.conbuildmat.2013.01.023.
[64] Ge TS, Dai YJ, Wang RZ. Review on solar powered rotary desiccant wheel cooling system. Renew Sustain Energy Rev 2014;39:476–97. https://doi.org/10.1016/j.rser.2014.07.121.
[65] Angrisani G, Roselli C, Sasso M. Experimental assessment of the energy performance of a hybrid desiccant cooling system and comparison with other air-conditioning technologies138; 2015. p. 533–45.

Nomenclature

A: area (m^2)
A: annuity ($/year)
c: coefficient (−)
c_p: specific heat capacity J/kgK
C: thermal capacitance (J/mK)
COP: coefficient of performance (−)
h: specific enthalpy (J/kg)
I: solar radiation (W/m^2)
k: thermal transmittance coefficient (W/m^2K)
$\dot{m}$: mass flow rate (kg/s)
P: electrical power (kW)
p: pressure (Pa)
q: equilibrium water content (kg/kg)
Q: thermal energy (J)
$\dot{Q}$: thermal power (W)
R: thermal resistance (mK/W)
SER: seasonal efficiency rate (−)
t: temperature (°C)
T: temperature (K)
U: internal energy (J)
V: volume (m^3)
$\dot{V}$: volume flow (m^3/h)
W: electrical energy (J)
w: air humidity ratio (g/kg)
z: depth (m)
Δ: difference (−)
ε: efficiency (−)
η: effectiveness parameter / efficiency (−)
λ: thermal conductivity (W/mK)
ρ: density (kg/m^3)
τ: time (s)
θ: phase shift of max. temperature (−)
$\varnothing$: generic quantity (−)
φ: relative humidity (%)

Subscripts and abbreviations

A: ambient
Amp: amplitude (monthly averages)
AC: air cooler
AH: air heater
C: condenser
Ch: chiller
gb: grout to borehole wall
BHX: borehole heat exchanger
C: cooling
CC: cooling ceilings
d: degradation
DW: desiccant wheel
E: evaporator
EHA: exhaust air
el: electrical
ETA: extract air

fg: fluid to grout
g: grout
gg: grout to grout
gv: grout vertical
h: enthalpy
HRW: heat recovery wheel
in: inlet
lat: latent
LC: life cycle
meas: measured
n: nominal
ODA: outdoor air
p: period
P: pump
PLR: part load ratio
pro: process air
reg: regeneration air
s: soil
sen: sensible
sv: soil vertical
SC: solar collector
sim: simulated
SUP: supply air
T: tank
t: total
th: thermal
TL: tank loop
v: vaporization
vl: violated
VCC: vapor compression cycle
w: water
WAHX: water-air heat exchanger
win: window
z: depth
0: yearly